Characterizing urban seismic noise recorded by distributed acoustic sensing array

Junzhu Shen and Tieyuan Zhu, Pennsylvania State University*

Summary

Ambient noise interferometry is based on the assumption of normally distributed noise sources, which is often hard to be satisfied in urban areas where local noise sources may be dominant in specific directions and times. Hence, understanding the characteristics of urban seismic noises is important to extract reliable surface waves for urban monitoring. In this study, we characterize urban seismic noise sources using a distributed acoustic sensing (DAS) fiber-optic array deployed in the city of State College, PA. We analyze spatial variation of background noise between off-campus areas and the main campus. We particularly show discovered wind-induced signals at resonant frequencies of 0.6 and 1.2 Hz and rain-induced signals at broadband frequencies (1 - 110 Hz). We also discover the distinct DAS recordings of three road-fiber geometries. The characteristics of different noise sources we reported will be expected to provide clues when conducting ambient noise interferometry of these DAS recordings.

Introduction

Urbanization is taking place across the world. Cities are expanding extremely fast with concentrations of people and wealth. Subsurface monitoring in urban cities is important to various fields, including subsurface engineering problems, geohazard investigation, and resource management. However, it is very challenging to conduct conventional geophysical surveys in populated areas due to location and cost limitations.

Recent studies demonstrate the application of long-term seismic monitoring using ambient noise interferometry with fiber-optic cable interrogated by distributed acoustic sensing (DAS) (Dou et al., 2017; Ajo-Franklin et al., 2019). Even more promising, DAS can turn existing telecommunication fiber into dense seismic sensor arrays with low-cost and low-maintenance (Martin et al., 2017). This idea of using telecommunication fiber for seismic monitoring has been demonstrated in several cities, including State College PA (Zhu et al., 2021), Los Angeles (Wang et al., 2020), and Bern (Smolinski et al., 2020). With dense recordings provided by DAS, the profile of surface waves can be retrieved using ambient-noise interferometry without active seismic surveys (Dou et al., 2017; Ajo-Franklin et al., 2019).

Ambient noise interferometry requires normally and uncorrelated distributed ambient noises (Wapenaar et al., 2010). This assumption is often hard to be satisfied in urban areas due to complicated anthropogenic noise wavefields from human activities. There are still some questions that remain unknown. First, we need to identify the noise sources we can use. Most previous studies use traffic noise from passing vehicles on the highways or trains on the track (Dou et al., 2017; Ajo-Franklin et al., 2019), limiting the study areas. For study areas away from busy roads, traffic noise might be too weak to be considered as dominant noise sources. Characterizing dominant noise sources along the fiber can help evaluate if the retrieved surface waves are reliable. Second, we need to characterize the local noise and remove these noises. Strong local noise from specific sources might violate the assumption of normal distribution of noise sources. Consequently, these noises, if not corrected, could likely cause the disturbance to interferometry data and further result in artifacts in surface wave estimations.

In this study, we aim at identifying the major noise sources in State College, PA. We use the seismic data continuously collected by a 4-km-long telecommunication fiber optic array deployed beneath the Penn State campus (Figure 1). We analyze spatial variation of background noise between off-campus areas and the main campus. We further identify signals generated by wind, rain and traffic. Finally, we expect that characterizing urban noises in detail can guide the design of passive surveys and help evaluate the performance of proposed ambient noise interferometry.

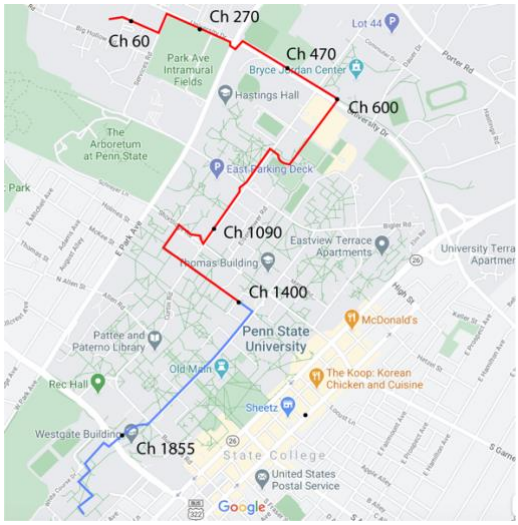

Figure 1: DAS array maps. Red line and blue line represent two fibers spliced together at Ch 1400.

Characterizing urban seismic noise

Data description

The continuous data we used were collected by the Penn State Fiber-Optic For Environment Sensing (FORESEE) array using underground telecommunication fiber optic cables. The DAS array makes continuous strain rate measurements at a 500 Hz sampling frequency with a 10 m gauge length and 2 m channel spacing, leading to all 2137 sensors. The fibers pictured in Figure 1 are sitting in a buried concrete conduit at a depth of roughly 1-meter underneath State College, PA. The fiber extends from less populated areas to the main campus, leading to highly spatial-varying background noise wavefields. The fiber distribution allows us to fully characterize the seismic noise in various locations. The details of the DAS array installation and calibration can be found in the paper (Zhu et al., 2021).

Observation of background noises

Figure 2 shows 1-min data at late night with no detected human activities. We observe clear spatial variation between off-campus areas and the main campus. There are many empty sport fields and agriculture in off-campus areas (Ch 1-600), making the amplitudes relatively low. In contrast, even though there is no traffic at midnight, strong background noise still exists on the main campus (Ch 600-1400). This consistently strong noise is likely caused by the utility. The piping system is concentrated in the main campus and the steam lines are next to the fiber-optics. Note that the attenuated laser signals after passing the fiber-optic connector at Ch 1400 cause the drop of amplitudes.

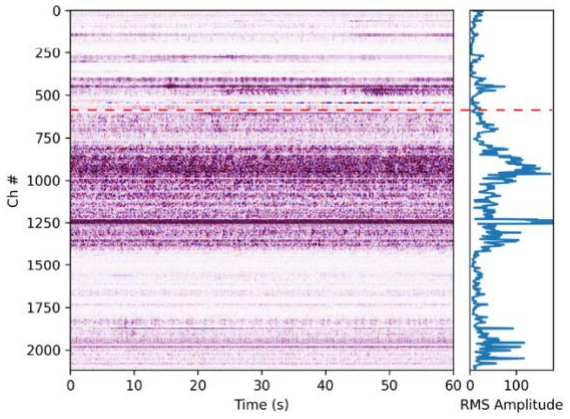

Figure 2: One-minute raw DAS recordings during 2:00-2:01 am, Nov 18, 2020 (left) and corresponding RMS amplitudes at each channel (right). Red dashed line represents the amplitude increase at Ch 600.

Next, we look at the frequency content of the background noise. We choose two data sections in off-campus areas (Ch170-270) and main campus (Ch845-945) (Figure 3a and 3c). The spectrum plot in Figure 3b shows that background noise in off-campus areas is weak in the cultural noise frequency band (< 25 Hz). The distribution of DAS measurements shows narrow Gaussian distribution (σ=22), indicating that the background noise is low-amplitude white noise from the instrument (Dumont et al., 2021). On the main campus, the dominant frequency band of seismic noise is 10-30 Hz (Figure 3d), which seems to be consistent with the low-frequency range of 2.5-30 Hz of piping system noises (Kostarev et al., 2007).

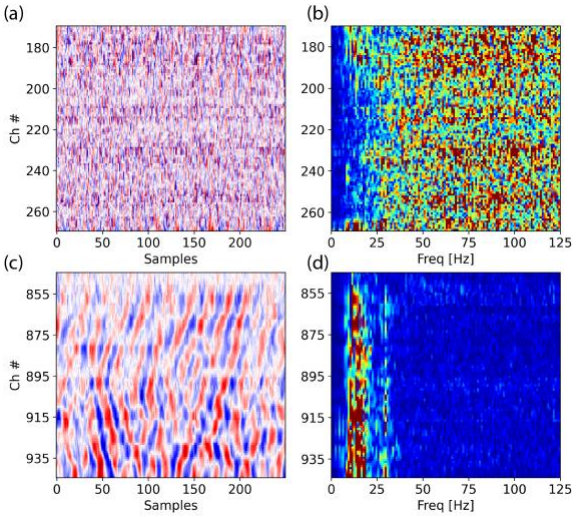

Figure 3: Background noise and corresponding spectrums at Ch 170-270 (a, b) and Ch 845-945 (c, d).

Characteristics of different noise sources

In this section, we show the characteristics of environmental noise (wind and rainfall) and traffic noise.

Wind

We examine DAS data at Ch 470 close to several big trees. We first calculate power spectra densities (PSD) for each hour every weekend from September to December 2020. The temporal variations of PSD (Figure 4a) show clear diurnal patterns in the frequency band above 8 Hz and the PSD seems to become stronger after Nov 07. It is interesting to note that we observe energy frequently occurred at the resonant frequencies of 0.6 and 1.2 Hz. Kerzenmacher and Gardiner (1998) reported that the tree roots swaying in the wind could generate signals in resonant frequencies at 0.48 and 1.3 Hz. They also pointed out that such resonant frequencies can be varying with the shape and the elasticity of the tree. We posit that such signals we observed are highly possible wind-generated signals.

We further validate our results with hourly wind speed data recorded by a weather station in State College. We calculate hourly seismic energy in the frequency band of 0.1-1 Hz and compare it with hourly wind speed data (Figure 4b). Not surprisingly, we can find a strong linear correlation with a coefficient of 0.8.

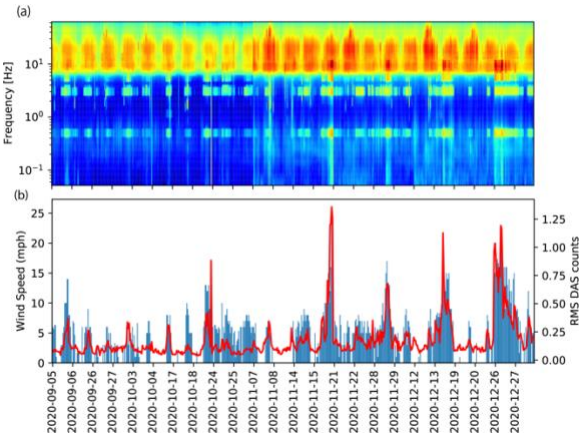

Figure 4: (a) Temporal variations of spectrums of recordings at Ch 470 from Sep 05 to Dec 27 2020. (b) Hourly RMS amplitudes in the frequency band of 0.1-1 Hz recorded at Ch 470 (red line) overlain hourly wind speed data (blue bars).

Rain

Because anthropogenic noise is generally very weak at night (see Figure 2), we expect to see rain-induced signals at certain frequency bands when it is rainy. Based on local weather records, on October 29, 2021, there was light rain starting around 3:15 am and rain became heavier after 4:35 am. Note that the times here could be shift in minutes because the observations were updated in every 20 minutes from the weather station.

We inspected the data recorded in off-campus areas (Ch 1-600). Figure 5a shows raw seismic recordings averaged among Ch 59-65 during the first three hours of the rain (3-6 am, local time). These channels are in a quiet area with a telecom hole just above the cable. The strong signals can be clearly seen after 4:35 am, which is highlighted as low frequencies in the time-frequency spectrum shown in Figure 5c. These signals (below 10 Hz) seem to appear after 4 am. After 5 am, These signals between 1 and 10 Hz, as well as some frequencies (18-24 Hz), become stronger. Clearly, there is a delay between the occurrence of signals and the start time of the rain. We interpret that when water accumulates on the ground surface and then flows down to the sewers, the pressure from the turbulent fluid flow to the sewer base or fluid-air interaction in the sewers could generate these low-frequency signals (0.5-10 Hz) as similar seismic observations during the river discharge (Schmandt et al., 2013). When the rain is light, there is not much water flowing into the sewerage; thus, the signals are weak. In contrast, when the rain becomes heavier, the fast-flowing water can generate strong signals. Figure 5b shows normalized RMS amplitudes of bandpass filtered seismic recording (filtered to 1-10 Hz). The peak (orange line) around 5:10 am is 40 minutes later than the start of heavy rain. This finding may link to river-discharge-induced signals during the rainfall episode (Diaz et al., 2014), which are in the 2.5-10 Hz frequency band.

We also note that there are some strong spikes up to 110 Hz (Figures 5a and 5c). These signals are likely generated by direct raindrops or possibly the existing metal electric box above the fiber shaking due to raindrops. The electric box may act as an amplifier when hit by raindrops.

We have to point out that not all channels show signals during rain. One possible reason is that rain-generated signals are too weak to penetrate to the fiber in the 1-m depth. Dean (2017) reported that burying the receivers is effective at reducing rain noise and rain noise is almost entirely attenuated at a depth greater than 0.3 m. Our fiber is at the depth of 1-m, which is likely to explain the absence of rain-induced signals in most of the areas.

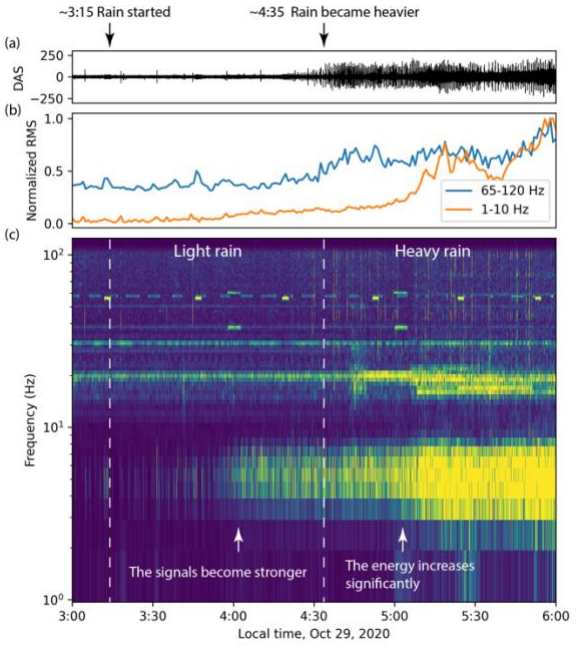

Figure 5: (a) Raw DAS data averaged from Ch 59-65. (b) Normalized RMS amplitudes at each minute. (c) Time-frequency spectrum of the trace shown in (a).

Traffic

Traffic signals are the most common sources in urban areas. However, the recorded traffic signals can be highly variable

because of different array orientations. Taking advantage of dense DAS sensors, we can characterize traffic signals from all three scenarios. Three fiber sections are selected: road-perpendicular fiber (Ch 1800-1950), road-over fiber (Ch 950-1150) and road-parallel fiber (Ch 350-450) (Figure 6).

For the signals at road-perpendicular fiber sections (Figure 6a), we observe strong surface waves at Ch 1874 propagating along the fiber. The surface waves can be detected within this 300 m section in the frequency band of 10-40 Hz. Passing vehicle acts as a point source at the cross point between road and fiber (Ch 1874). The RMS amplitudes at each channel confirm the geometric spreading of a single source: the energy decays with the offset increase.

We then show the recordings of a car driving right above the fiber (Figure 6b). The streak in the seismogram indicates the car moving. The surface waves generated by the car decay quickly and can only be detected in the range of 20 nearby channels. The spectrum shows traffic signals contain not only the surface waves generated by the car (10-40 Hz) but also strong low-frequency signals (<2 Hz). The low-frequency signals, which don't appear in the other two fiber sections, are likely generated by the quasi-static deformation caused by the car's weight (Yuan et al., 2020). The flat RMS-versus-offset curve indicates that the wavefield is composed of different sources along the road.

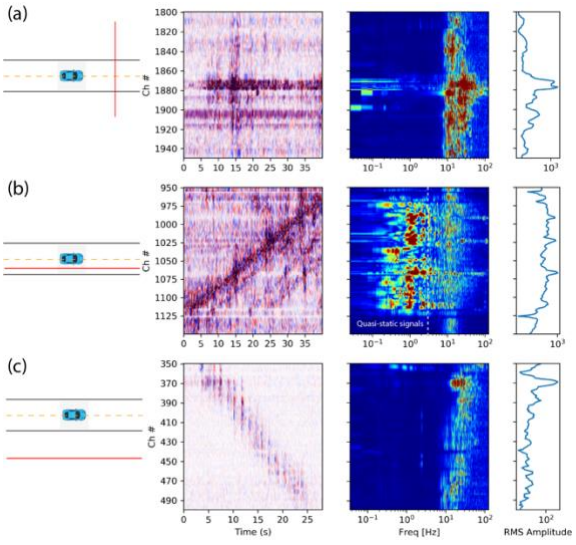

Figure 6: Examples of traffic signals recorded by three fiber sections: (a) road-perpendicular fiber, (b) road-over fiber, and (c) road-parallel fiber. From left to right: (1) sketch about road-fiber geometry, (2) Raw DAS recordings, (3) Corresponding frequency spectrums at each channel and (4) RMS amplitudes along the fiber.

The third data recorded at the road-parallel fiber section shows similar characteristics with the road-over fiber section, except for the absence of low-frequency quasi-static signals (Figure 6c). Moreover, the spectrum shows that the dominant frequency decreases along the fiber. This is likely caused by distance changes between fiber and road. Due to the topography, the fiber is not precisely parallel to the road. The fiber at the side of Ch 350 may be closer to the road than the other end, which results in the decreasing RMS amplitudes along the fiber. The shorter source-receiver offset enables the detection of higher-frequency surface waves up to 40 Hz. For Ch 450, high-frequency signals might attenuate during the propagation in longer distance, resulting in a lower dominant frequency (<30 Hz).

Ideally, we prefer the car-generated surface waves propagating along the fiber direction to better retrieve seismic waves. Our results show that road-perpendicular fiber is most sensitive to traffic signals, which provide opportunities for retrieving coherent surface waves.

Conclusions

We report urban seismic noise recorded by a telecommunication fiber array. In particular, we observe clear wind-generated noise at the frequency of 0.6 and 1.2 Hz, possibly due to the swaying of tree roots. During the rain, seismic signals are enhanced in a broad frequency band (1-110 Hz). According to the variations in time and frequency, we attribute the 1-10 Hz signals to the interaction between accumulated water and air/sewer bases. The spikes up to 110 Hz during heavy rain might be caused by direct raindrops or an electric box shaking in the rain. We further show the characteristics of traffic signals in different scenarios, which can help map the location of dark fibers in the future urban study. Our results could help future urban studies evaluate what urban seismic noise might appear in their recordings. Further analysis will be applied across the array for a detailed spatial distribution. Furthermore, our results provide insight into various applications, including environmental monitoring, traffic monitoring and geohazard investigation.

Acknowledgement

We thank Eileen Martin for helpful discussion on this work. The DAS array was supported by Penn State Institute of Environment and Energy seed grant and Institute of Natural Gas Research. The wind speed data and weather history information were obtained from: wunderground.com/history (last accessed on March 28, 2021).

REFERENCES

Ajo-Franklin, J. B., S. Dou, N. J. Lindsey, I. Monga, C. Tracy, M. Robertson, V. R. Tribaldos, C. Ulrich, B. Freifeld, T. Daley and X. Li, 2019, Distributed acoustic sensing using dark fiber for near-surface characterization and broadband seismic event detection: Scientific Reports, **9**, no. 1, doi: https://doi.org/10.1038/s41598-018-36675-8.

Dean, T., 2017, The seismic signature of rain: Geophysics, **82**, no. 5, P53–P60, doi: https://doi.org/10.1190/geo2016-0421.1.

Díaz, J., M. Ruíz, L. Crescentini, A. Amoruso, and J. Gallart, 2014, Seismic monitoring of an Alpine mountain river: Journal of Geophysical Research: Solid Earth, **119** no. 4, 3276–3289, doi: https://doi.org/10.1002/2014jb010955.

Dou, S., N. Lindsey, A. M. Wagner, T. M. Daley, B. Freifeld, M. Robertson, J. Peterson, C. Ulrich, E. R. Martin, and J.B. Ajo-Franklin, 2017, Distributed acoustic sensing for seismic monitoring of the near surface: a traffic-noise interferometry case study: Scientific Reports, **7**, no. 1, 11620, doi: https://doi.org/10.1038/s41598-017-11986-4.

Dumont, V., V. R. Tribaldos, J. Ajo-Franklin, and K. Wu, 2021, Deep learning for surface wave identification in distributed acoustic sensing data: Arxiv.Org. http://arxiv.org/abs/2010.10352.

Kerzenmacher, T., and B. Gardiner, 1998, A mathematical model to describe the dynamic response of a spruce tree to the wind: Trees, **12**, no. 6, 385, doi: https://doi.org/10.1007/s004680050165.

Kostarev, V., A. Tuomas and K-H. Reinsch, 2007, Resolving of steam and feed-water piping vibration matter at Loviisa NPP: 19th International Conference on Structural Mechanics in Reactor Technology, Conference Paper.

Martin, E. R., C. M. Castillo, S. Cole, P. S. Sawasdee, S. Yuan, R. Clapp, M. Karrenbach, and B. L. Biondi, 2017, Seismic monitoring leveraging existing telecom infrastructure at the SDASA: active, passive, and ambient-noise analysis: The Leading Edge, **36**, 12, 1025–1031, doi: https://doi.org/10.1190/tle36121025.1.

Schmandt, B., R. C. Aster, D. Scherler, V. C. Tsai, and K. Karlstrom, 2013, Multiple fluvial processes detected by riverside seismic and infrasound monitoring of a controlled flood in the Grand Canyon: Geophysical Research Letters, **40**, no. 18, 4858–4863, doi: https://doi.org/10.1002/grl.50953.

Smolinski, K., P. Paitz, D. Bowden, P. Edme, F. Kugler, and A. Fichtner, 2020, Urban distributed acoustic sensing using in-situ fibre beneath Bern, Switzerland: doi:https://doi.org/10.5194/egusphere-egu2020-8225.

Wang, X., E. F. Williams, M. Karrenbach, M. G. Herráez, H. F. Martins, and Z. Zhan, 2020, Rose parade seismology: signatures of floats and bands on optical fiber: Seismological Research Letters, **91**, no. 4, 2395–2398, doi: https://doi.org/10.1785/0220200091.

Wapenaar, K., D. Draganov, R. Snieder, X. Campman, and A. Verdel, 2010, Tutorial on seismic interferometry: Part, 1.
— Basic principles and applications: Geophysics, **75**, no. 5, 75A195–75A209, doi: https://doi.org/10.1190/1.3457445.

Yuan, S., A. Lellouch, R. G. Clapp, and B. Biondi, 2020, Near-surface characterization using a roadside distributed acoustic sensing array: The Leading Edge, **39**, no. 9, 646–653, doi: https://doi.org/10.1190/tle39090646.1.

Zhu, T., J. Shen, and E. R. Martin, 2021, Sensing earth and environment dynamics by telecommunication fiber-optic sensors: an urban experiment in Pennsylvania, USA: Solid Earth, **12**, no. 1, 219–235, doi: https://doi.org/10.5194/se-12-219-2021.